HVAC&R Research

ISSN: 1078-9669 (Print) 1938-5587 (Online) Journal homepage: http://www.tandfonline.com/loi/uhvc20

An Inverse Gray-Box Model for Transient Building Load Prediction

James E. Braun & Nitin Chaturvedi

To cite this article: James E. Braun & Nitin Chaturvedi (2002) An Inverse Gray-Box Model for Transient Building Load Prediction, HVAC&R Research, 8:1, 73-99

To link to this article: https://doi.org/10.1080/10789669.2002.10391290

Published online: 03 Mar 2011.

An Inverse Gray-Box Model for Transient Building Load Prediction

James E. Braun, Ph.D.
Member ASHRAE

Nitin Chaturvedi

Lower costs and improved performance of sensors, controllers, and networking is leading to the development of smart building features, such as continuous performance monitoring, automated diagnostics, and optimal supervisory control. For some of these applications, it is important to be able to predict transient cooling and heating requirements for the building using inverse models that are trained using on-site data. Existing inverse models for transient building loads range from purely empirical or "black-box" models to purely physical or "white-box" models. Generally, black-box (e.g., neural network) models require a significant amount of training data and may not always reflect the actual physical behavior, whereas white-box (e.g., finite difference) models require specification of many physical parameters. This paper presents a hybrid or "gray-box" modeling approach that uses a transfer function with parameters that are constrained to satisfy a simple physical representation for energy flows in the building structure. A robust method is also presented for training parameters of the constrained model, wherein initial values of and bounds on physical parameters are estimated from a rough building description, better estimates are obtained using a global direct search algorithm, and optimal parameters are identified using a nonlinear regression algorithm. The model and training method were extensively tested for different buildings and locations using data generated from a detailed simulation program. The approach was also tested using data from a field site located near Chicago, Illinois. It was found that one to two weeks of data are sufficient to train a model so that it can accurately predict transient cooling or heating requirements.

INTRODUCTION

The 2001 *ASHRAE Handbook—Fundamentals* breaks modeling into two basic categories: *forward* modeling and *inverse* modeling. Forward modeling generally begins with a physical description of the building. This can include the building's construction materials, geometry, geographic location, and the type of HVAC system. This type of model is typically used for design of a HVAC system. Inverse models are derived from empirical behavior and are expressed in terms of one or more driving forces and a set of empirical parameters. A model form is assumed and measured data are used to "back out" the parameters that provide the most accurate representation for the chosen model form and data set. Also referred to as system identification, this type of model can be used for retrofit analysis, performance monitoring and diagnostics, control strategy development, and on-line control applications.

Figure 1 is a schematic of a cooling system for a typical building. The major components of the system are the building, the cooling plant, and the air distribution system. In order to predict overall energy requirements, it is necessary to have a model for the cooling required to maintain temperature and humidity of the air within the building.

James E. Braun is a professor and **Nitin Chaturvedi** is a graduate student in the School of Mechanical Engineering, Ray W. Herrick Laboratories, Purdue University, West Lafayette, Indiana.

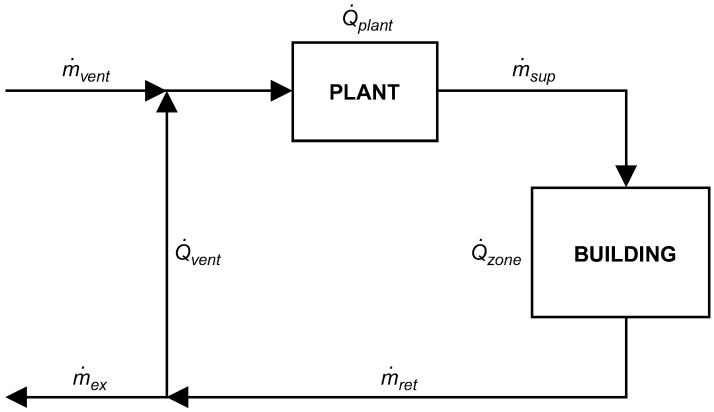

Figure 1. Thermal System for Building Cooling

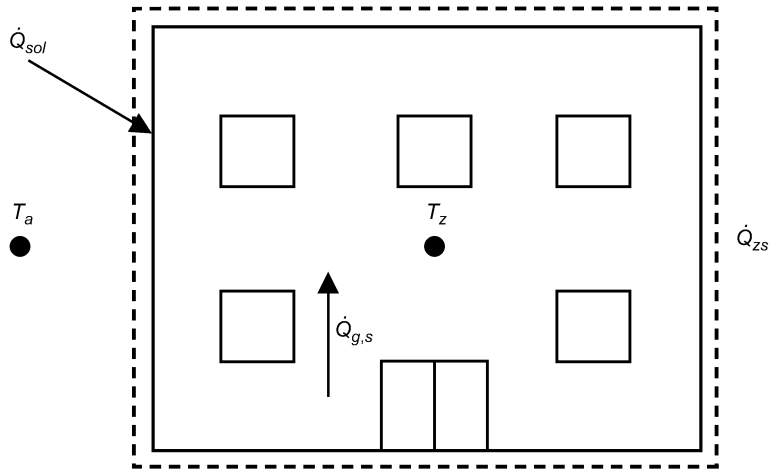

Figure 2. Schematic of Major Thermal Influences on Zone Sensible Load

The cooling requirement for any zone within a building ($\dot{Q}_{zone}$) can be separated into latent and sensible contributions. Latent heat gains are associated with the addition of water vapor into the air, which must ultimately be removed by the plant. In building zones, latent gains are primarily due to occupant respiration, infiltration of moist, ambient air, and aesthetic sources such as organic plants and fountains. Although latent loads associated with ventilation may be significant, zone latent loads are a minor portion of the total zone load and are often modeled using a steady-state moisture balance with moisture gains that are proportional to the number of occupants.

Figure 2 shows a schematic representation of the major influences on the sensible zone load. Sensible zone loads ($\dot{Q}_{zs}$) are due to heat transfer from "warm" surfaces within the zone. The sources of these gains can be both internal and external to the building. Typical internal sources ($\dot{Q}_{gs}$) are occupants, lights, and equipment (computers, copy machines, etc.). External sources for heat gains include solar radiation ($\dot{Q}_{sol}$) transmitted through windows and absorbed on external walls and energy conduction through external walls and windows due to the difference between the ambient and space temperatures.

The sensible zone loads are much more difficult to model than latent loads. There are many different paths for heat transfer, and transient effects are very important. This paper describes the development and evaluation of an inverse model for the sensible zone loads that was developed as a tool to evaluate strategies for using building thermal mass (Braun et al. 2001).

A variety of different approaches have been proposed for inverse modeling of building sensible loads (see Crabb et al. 1987; Haghighat et al. 1988; Rabl 1988; Athienitis and Shou 1990; Braun 1990; Balaras 1996). The models include thermal networks, modal analysis, differential equations, autoregressive moving average (ARMA) models, Fourier series, calibrated computer simulations, and transfer functions. Inverse modeling has also been applied to the more general problem of predicting total building energy consumption. In particular, a number of papers (MacKay 1994; Ohlsson et al. 1994; Feuston and Thurtell 1994; Stevenson 1994; Iijima et al. 1994; Kawashima 1994) described the results of a competition called the "Great Energy Predictor Shootout." The participants trained black-box models using four months of hourly data from late fall and early winter and then tested the models using a month of data in the middle of winter. The most successful modeling approaches used artificial neural networks with a time history of weather data as inputs.

The most difficult part of the model development for a particular application is the process of identifying the model order and the optimum parameters. Applying regression techniques to "black-box" approaches, such as ARMA, transfer function, or neural network models, can lead to models that do not respect the proper physics (e.g., high-frequency dynamic oscillations not present in the real system). It is generally necessary to acquire data over a long period of time with widely varying conditions in order to train black-box models that can provide accurate predictions, or even trends, under all conditions. For instance, the black-box models used for the "Great Energy Predictor Shootout" were trained with four months of data and yet the errors associated with the one-month testing period were larger than those associated with the training period. Furthermore, it is not known how well the models would perform in predicting building energy use if there were a major change in the control strategies employed, such as would occur in going from a night setup control to a precooling control strategy.

At the other extreme, purely physical or "white-box" models can predict the effects of changes in control strategies quite well. However, they use many parameters that must either be known from a detailed description of the building or tuned with experimental data. The process of collecting a physical description is time consuming and probably not cost effective. The process of tuning the parameters of a physical model is difficult with the limited sensor information that is generally available.

The goal of the work described in this paper was to develop a modeling and parameter estimation approach for building sensible cooling requirements that would (1) allow model training using a limited number of sensors with data acquired over a short period of time (with night setup control in place) and (2) would then allow accurate predictions associated with the use of different precooling strategies for the building (see Braun et al. 2001). The resulting model is a hybrid or "gray-box" approach that uses a transfer function model with parameters that are constrained to satisfy a simple physical representation for energy flows in the building structure. A unique three-step process was developed for learning the optimal parameters:

1. Bounds on physical parameters are estimated from a rough description of the building geometry and materials.
2. A global direct search algorithm is used to determine estimates of the model parameters that satisfy the constraints on parameters and the physical representation.

3. A nonlinear regression algorithm that relies on local derivative information is used to determine optimal parameters that minimize errors between model predictions and measurements and satisfy the constraints.

Optimization methods that rely solely on derivative information can find local minima if the initial guesses are not chosen well. In the global search, the search for an optimum occurs over the entire feasible parameter space and a discrete set of cost function evaluations are performed for specified points within the chosen parameter space. This approach finds a "coarse" optimum with a resolution dictated by the number of points chosen for the search and within parameter bounds based upon a physical description of the problem. The specific points for the global search are located within the parameter space using an algorithm that minimizes the dispersion of the generated set. The best point from the global search is then used as the initial guess for a local optimization method that uses derivative information. In effect, the global algorithm finds a coarse solution and the local method "fine-tunes" the result. As a result, a relatively small number of points are needed for the direct search and yet the method is much more likely to find the global minimum as compared with the use of a local optimization method alone.

Both detailed physical models and measurements were used in the development and validation of the hybrid inverse model. Data generated by finite-difference solutions to a detailed physical model of different walls were used in identifying the proper model order for the simplified model. Data generated by a detailed physical model of different zones were used in studying the impact of different training scenarios on the ability of the model to predict loads for separate test periods. Finally, measurements from a field site were used to evaluate the actual performance of the modeling approach.

Model Foundation

The building model developed in this study is based upon the work of Braun (1990) and Seem et al. (1989). For a given time step, Braun presented the following transfer function for estimating the sensible cooling required to keep the zone temperature at a given set point:

$$\dot{Q}_{zs,k} = \sum_{i=0}^{N} (a_i T_{a,k-i} + b_i T_{z,k-i} + c_i \dot{Q}_{g,s,k-i} + d_i \dot{Q}_{sol,k-i}) + \sum_{i=1}^{M} e_i \dot{Q}_{zs,k-i} \quad (1)$$

This transfer function model relates the zone sensible load at a given time to current and previous values of the major inputs, as well previous values of the zone sensible load. Through mathematical manipulation, the zone temperature at a given time can be determined as

$$T_{z,k} = \frac{1}{b_o}\left[\dot{Q}_{zs,k} - \sum_{i=1}^{M} e_i \dot{Q}_{zs,k-i} - \sum_{i=0}^{N} (a_i T_{a,k-i} + c_i \dot{Q}_{g,s,k-i} + d_i \dot{Q}_{sol,k-i}) - \sum_{i=1}^{N} b_i T_{z,k-i}\right] \quad (2)$$

This allows the building zone temperature to be determined during "floating" periods, or periods when the cooling system is off.

Braun (1990) applied direct nonlinear regression to determine the coefficients of Equation (1) that minimize prediction errors for data generated from detailed physical models for different building specifications. The model matched the detailed simulation results for transient cooling and heating requirements within about 2% when trained using a year's worth of hourly results with "rich" variations in zone temperature. Montgomery (1998) investigated similar model

forms and studied additional simulated buildings and training strategies with hourly time steps. He found that at least 21 days of training data were needed to achieve root-mean-square (RMS) errors of between 2 and 4% of the peak loads using a control strategy that varied the zone temperature set points during occupied and unoccupied times. However, the model produced some high-frequency dynamic oscillations that were not present in the data.

The goal of the work presented in this paper was to modify the transfer function model and training approach to

- Reduce the amount of required training data
- Allow the use of a conventional control strategy for zone temperature variations (e.g., night setup) for training
- Eliminate high-frequency oscillations in the predicted loads.

This was accomplished by constraining transfer function coefficients to satisfy a simple state-space representation for the building.

A general state-space model for estimating sensible zone loads is of the form

$$\frac{d\mathbf{x}}{d\tau} = \mathbf{A}\mathbf{x} + \mathbf{B}\mathbf{u} \tag{3}$$

$$y = \mathbf{c}^T\mathbf{x} + \mathbf{d}^T\mathbf{u} \tag{4}$$

For a building model, the output variable is the rate of heat transfer to the air within the building (i.e., the sensible zone load). The state vector contains temperatures of "nodes" within the structure of the building. The appropriate number of states to use in representing a building is an important consideration and is addressed in subsequent sections. The input vector includes all of the important driving conditions, such as zone temperature, ambient temperature, incident solar radiation, and internal gains.

Seem et al. (1989) presented a technique for determining an equivalent transfer function representation from the state-space representation that involves the exact solution to the set of first-order differential equations with the inputs modeled as continuous, piecewise linear functions. The solution for the output at any time t is of the form

$$y(t) = \sum_{k=0}^{N_{state}} \mathbf{S}_k^T \mathbf{u}_{t-k\Delta\tau} - \sum_{k=1}^{N_{state}} e_k y(t - k\Delta\tau) \tag{5}$$

The vectors $\mathbf{S}_k$ for $k = 0$ to N_{state} are determined as

$$\begin{aligned} \mathbf{S}_0 &= \mathbf{c}\mathbf{R}_0\Gamma_2 + \mathbf{d} \\ \mathbf{S}_j &= \mathbf{c}[\mathbf{R}_{j-1}(\Gamma_1 - \Gamma_2) + \mathbf{R}\Gamma_2] + e_j\mathbf{d} \qquad \text{for } 1 \le j \le (N_{state} - 1) \\ \mathbf{S}_{N_{state}} &= \mathbf{c}\mathbf{R}_{N_{state}-1}(\Gamma_1 - \Gamma_2) + e_{N_{state}}\mathbf{d} \end{aligned} \tag{6}$$

where

$$\begin{aligned} \Gamma_1 &= \mathbf{A}^{-1}(\Phi - \mathbf{I})\mathbf{B} \\ \Gamma_2 &= \mathbf{A}^{-1}\left(\frac{\Gamma_1}{\Delta\tau} - \mathbf{B}\right) \end{aligned} \tag{7}$$

where $\mathbf{I}$ is the identity matrix, $\Delta\tau$ is the simulation time step (one hour for this study), and

$$\begin{aligned} \Phi &= e^{\mathbf{A}\Delta\tau} \\ e^{\mathbf{A}\Delta\tau} &= \mathbf{I} + \mathbf{A}\Delta\tau + \frac{\mathbf{A}^2(\Delta\tau)^2}{2!} + \frac{\mathbf{A}^3(\Delta\tau)^3}{3!} + \cdots + \frac{\mathbf{A}^n(\Delta\tau)^n}{n!} + \cdots \end{aligned} \tag{8}$$

Seem et al. (1989) presented an efficient algorithm for evaluating $e^{\mathbf{A}\Delta\tau}$ in Equation (8). The matrices $\mathbf{R}_j$ used in the determination of $\mathbf{S}_k$ and the e_j transfer function coefficients are determined recursively as

$$\begin{aligned} \mathbf{R}_0 &= \mathbf{I} & e_1 &= -\frac{Tr(\Phi\mathbf{R}_0)}{1} \\ \mathbf{R}_1 &= \Phi\mathbf{R}_0 + e_1\mathbf{I} & e_2 &= -\frac{Tr(\Phi\mathbf{R}_1)}{2} \\ \mathbf{R}_2 &= \Phi\mathbf{R}_1 + e_2\mathbf{I} & e_3 &= -\frac{Tr(\Phi\mathbf{R}_1)}{3} \\ &\vdots & &\vdots \\ \mathbf{R}_{N_{state}-1} &= \Phi\mathbf{R}_{N_{state}-2} + e_{N_{state}-1}\mathbf{I} & e_{N_{state}} &= -\frac{Tr(\Phi\mathbf{R}_{N_{state}-1})}{N_{state}} \end{aligned} \tag{9}$$

where $Tr(\ )$ is the trace of the matrix (the sum of the diagonal elements).

Model Order Evaluation

A typical building includes external walls (walls directly coupled to the ambient), internal walls (walls not directly coupled to the ambient), a roof/ceiling, and a floor. A systematic approach was followed to identify a good model representation for individual walls. As a baseline for comparison, a detailed physical model was developed based upon finite-difference solutions to partial differential equations that model conduction in a wall with convection boundary conditions. This model was used to generate predictions of heat-transfer rates at the inside surface for four different wall constructions. These data were used to train transfer function models of different order (i.e., different numbers of state variables) that satisfy the state-space representation presented in the previous section. The performances associated with the different model orders were then compared to identify an appropriate model form.

The state-space model can be represented using an electrical analog. Figure 3 shows a simple two-node representation (two state variables) for a hypothetical building wall subjected to time-varying temperature boundary conditions. The purpose of the model is to predict the heat-transfer rate to the air within the building ($\dot{Q}_i$). The total thermal resistance ($R_1 + R_2 + R_3$) includes the thermal convection resistance between the outside air and the wall, the conduction resistance within the wall and the thermal convection resistance between the wall and the building interior. The two capacitors should incorporate the total capacitance of the wall material. For this simple representation, the physical location of the nodes has a significant effect on the model predictions.

The electrical analog of Figure 3 is easily converted to the state-space model of Equation (5). In this case, the state vector contains the two nodal temperatures (T_1 and T_2), the input vector includes the outside and inside air temperatures (T_i and T_o), and the output variable is $\dot{Q}_i$. A transfer function model for $\dot{Q}_i$ can then be generated using the procedure presented in the previous section.

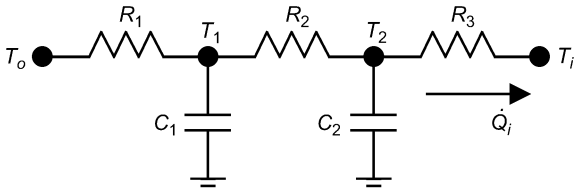

Figure 3. Thermal Network Representation of Hypothetical Building Wall

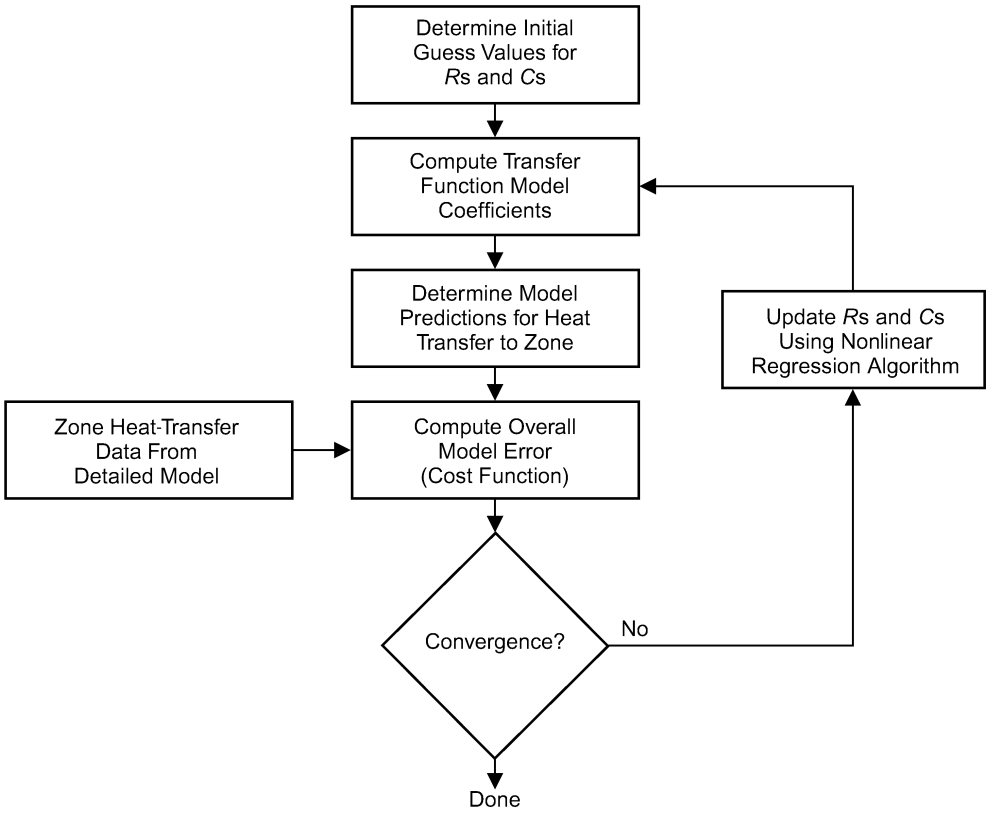

Figure 4. Flowchart for Training Transfer Function Wall Models

Figure 4 shows the process for learning appropriate values for resistances (*R*s) and capacitances (*C*s) used for the wall model order evaluation. Initial guess values of the *R*s were determined by dividing the total resistance (from a physical description of the walls) by the number of state variables plus one. Similarly, initial *C* values were taken as the total capacitance divided by the number of state variables. A regression algorithm was then applied to adjust the *R*s and *C*s to minimize errors between predictions of the simplified model and the detailed finite-difference model. At each iteration of the regression, the state-space solution presented in the previous section was used to determine a transfer function model.

During the regression process, the sum of the individual wall resistances and capacitances was constrained to be equal to the known values. Effectively, with this constraint in place, the location of the nodes was adjusted through adjustments in the individual *R*s and *C*s. The regression cost function was the integrated root-mean-square error defined as

Table 1. Wall Constructions For Different Sample Walls

Wall	Layer	Thickness		Conductivity		Specific Heat		Density	
		in	cm	Btu/(h·ft·°F)	W/(m·K)	Btu/(lb_m·°F)	kJ/(kg·K)	lb_m/ft^3	kg/m^3
External	Gypsum	5/8	1.59	0.098	0.17	0.24	1.0	50	801
	Insulation	1	2.54	0.017	0.029	0.29	1.21	2.2	35
	Block	4	10.1	0.417	0.721	0.21	0.88	60	961
	Brick	4	10.1	0.417	0.721	0.19	0.80	120	1922
	Plaster	5/8	1.59	0.133	0.230	0.25	1.05	37	593
Internal	Block	4	10.1	0.417	0.721	0.21	0.88	60	961
	Plaster	5/8	1.59	0.133	0.230	0.25	1.05	37	593
	Ceramic Tile	1/2	1.27	0.033	0.057	0.14	0.59	23	368
Ceiling	Concrete	2	5.08	0.433	0.749	0.21	0.88	120	1922
	Insulation	1	2.54	0.017	0.029	0.29	1.21	2.2	35
	Roof	3/8	0.95	0.093	0.161	0.35	1.47	70	1121
Floor	Carpet	1/2	1.27	0.03	0.052	0.33	1.38	35	561
	Tile	1/4	0.64	0.3	0.519	0.24	1.0	100	1602
	Concrete	4	10.1	0.433	0.749	0.21	0.88	120	1922

$$J = \sqrt{\frac{\sum_{k=1}^{N} \left(\dot{Q}_{i,m,k} - \dot{Q}_{i,d,k}\right)^2}{N-1}} \tag{10}$$

where N is the number of data points and the subscripts m and d denote simplified model predictions and data (detailed model results), respectively. The cost function is nonlinear in the unknown R and C parameters. A Levenberg-Marquardt algorithm (Marquardt 1963, Meyer 1970) was applied to minimize the cost function of Equation (10).

The four different wall constructions presented in Table 1 were considered in the model order evaluation. These descriptions are typical of an external wall, internal wall, ceiling/roof, and slab floor.

Figure 5 shows sample comparisons between the finite difference model and simplified two-node model predictions for the ceiling/roof description with a step change in outside temperature from 73 to 80°F (22.8 to 26.7°C) with a constant inside temperature of 73°F (22.8°C). Model predictions for heat transfer to the inside air are given for both the initial (unregressed) and optimal (regressed) values of the Rs and Cs. The two-node model does not work well if the individual Rs and Cs are distributed evenly (unregressed case). However, optimal positioning of the nodes does result in a very good model with small prediction errors.

Similar results were found for all four walls subjected to different time-varying inputs. The RMS errors normalized with the maximum heat flow were on the order of 0.5%. The regressed parameters, obtained under one set of input conditions, were also tested under different input conditions and provided similar accuracy. Both one-node and three-node representations were also investigated. One-node models were rejected due to higher RMS errors (about 2.5%), while three-node models did not provide significant improvement over the two-node ones.

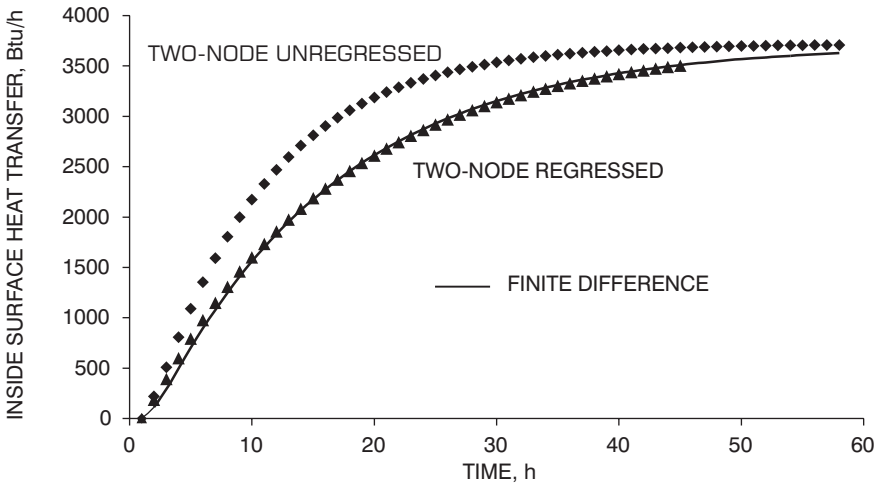

Figure 5. Comparisons of Inside Surface Wall Heat Transfer
(Ceiling with a Two-Node Representation)

Overall Building Model

Several different models were investigated for predicting the total heat gains to the zone air. Figure 6 depicts an electrical analog for a model that was found to work well under all situations investigated. Five different types of structures are considered: (1) external walls, (2) ceiling/roof, (3) floor, (4) internal walls, and (5) windows. The *T*s, *R*s and *C*s in Figure 6 denote temperatures, resistances, and capacitances with the subscripts *e*, *c*, *f*, *i*, *w*, *a*, *z*, *g* representing external, ceiling, floor, internal, window, ambient air, zone air, and ground, respectively. The zone temperature appears twice to make the diagram more readable, but corresponds to a single node. All of the structures, except the windows, are represented with two nodes. The windows have negligible energy storage and are represented with a pure resistance. The symbol $\dot{Q}_{sol}$ denotes total absorbed solar radiation on external surfaces with the subscripts *e* and *c* representing the external walls and the roof/ceiling, respectively. The solar radiation that is transmitted through windows, $\dot{Q}_{sol,w}$, is distributed evenly between the two nodes associated with the internal walls. Convective internal gains, $\dot{Q}_{g,c}$, are applied directly to the zone node, while the radiative internal gains are divided between the interior nodes of the ceiling/roof ($\dot{Q}_{g,r,c}$) and external wall ($\dot{Q}_{g,r,e}$) according to their relative surface areas. The internal gains are assumed to be 70% convective and 30% radiative. All resistances and capacitances are assumed to be time invariant. Thus, the effect of varying wind velocity on external convection coefficients is not considered.

The thermal network of Figure 6 can be represented with a state-space model of the form of Equation (5) with the following definitions for state, input, and output variables:

$$\mathbf{x}^T = [T_{c,1}\ T_{c,2}\ T_{e,1}\ T_{e,2}\ T_{f,1}\ T_{f,2}\ T_{i,1}\ T_{i,2}] \tag{11}$$

$$\mathbf{u}^T = [T_z\ T_a\ T_g \dot{Q}_{sol,c} \dot{Q}_{sol,e} \dot{Q}_{g,r,c} \dot{Q}_{g,r,e} \dot{Q}_{sol,w} \dot{Q}_{g,c}] \tag{12}$$

$$y = \dot{Q}_{sh} \tag{13}$$

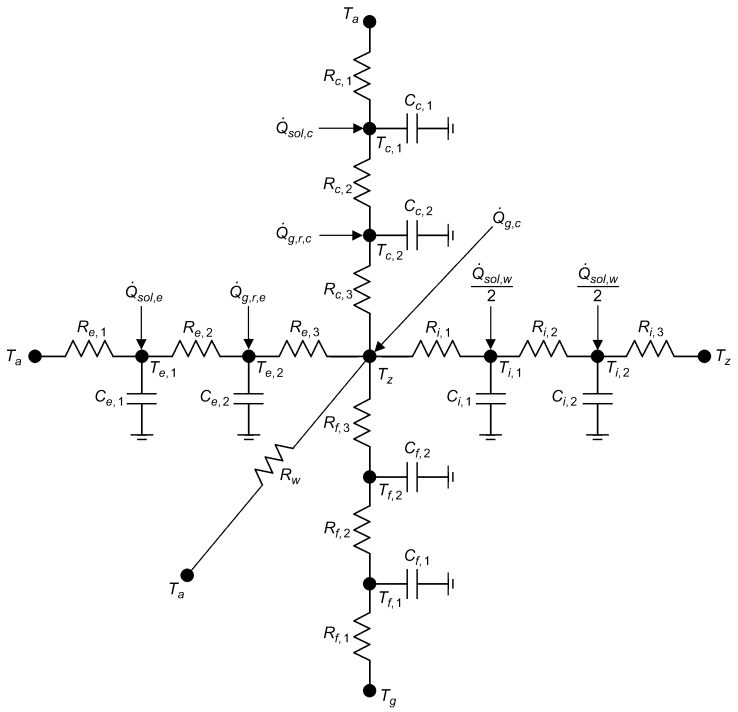

Figure 6. Thermal Network for Overall Building Model

where $\dot{Q}_{sh}$ is the instantaneous heat gain to the building air from all surfaces. For this model, the nonzero elements of the state-space coefficient matrices and vectors are

$$
\begin{aligned}
\mathbf{A}(1,1) &= \frac{-1}{R_{c,1}C_{c,1}} + \frac{-1}{R_{c,2}C_{c,1}} & \mathbf{A}(1,2) &= \frac{1}{R_{c,2}C_{c,1}} \\
\mathbf{A}(2,1) &= \frac{1}{R_{c,2}C_{c,1}} & \mathbf{A}(2,2) &= \frac{-1}{R_{c,2}C_{c,2}} + \frac{-1}{R_{c,3}C_{c,2}} \\
\mathbf{A}(3,3) &= \frac{-1}{R_{e,1}C_{e,1}} + \frac{-1}{R_{e,2}C_{e,1}} & \mathbf{A}(3,4) &= \frac{1}{R_{e,2}C_{e,1}} \\
\mathbf{A}(4,3) &= \frac{1}{R_{e,2}C_{e,2}} & \mathbf{A}(4,4) &= \frac{-1}{R_{e,2}C_{e,2}} + \frac{-1}{R_{e,3}C_{e,2}} \\
\mathbf{A}(5,5) &= \frac{-1}{R_{f,1}C_{f,1}} + \frac{-1}{R_{f,2}C_{f,1}} & \mathbf{A}(5,6) &= \frac{1}{R_{f,2}C_{f,1}} \\
\mathbf{A}(6,5) &= \frac{1}{R_{f,2}C_{f,2}} & \mathbf{A}(6,6) &= \frac{-1}{R_{f,2}C_{f,2}} + \frac{-1}{R_{f,3}C_{f,2}} \\
\mathbf{A}(7,7) &= \frac{-1}{R_{i,1}C_{i,1}} + \frac{-1}{R_{i,2}C_{i,1}} & \mathbf{A}(7,8) &= \frac{1}{R_{i,2}C_{i,1}} \\
\mathbf{A}(8,7) &= \frac{1}{R_{i,2}C_{i,2}} & \mathbf{A}(8,8) &= \frac{-1}{R_{i,2}C_{i,2}} + \frac{-1}{R_{i,3}C_{i,2}}
\end{aligned}
\tag{14}
$$

$$
\begin{aligned}
\mathbf{B}(1,2) &= \frac{1}{R_{c,1}C_{c,1}} \qquad \mathbf{B}(1,4) = \frac{1}{C_{c,1}} \\
\mathbf{B}(2,1) &= \frac{1}{R_{c,3}C_{c,2}} \qquad \mathbf{B}(2,6) = \frac{1}{C_{c,2}} \\
\mathbf{B}(3,2) &= \frac{1}{R_{e,1}C_{e,1}} \qquad \mathbf{B}(3,5) = \frac{1}{C_{e,1}} \\
\mathbf{B}(4,1) &= \frac{1}{R_{e,3}C_{e,2}} \qquad \mathbf{B}(4,7) = \frac{1}{C_{e,2}} \\
\mathbf{B}(5,3) &= \frac{1}{R_{f,1}C_{f,1}} \\
\mathbf{B}(6,1) &= \frac{1}{R_{f,3}C_{f,2}} \\
\mathbf{B}(7,1) &= \frac{1}{R_{i,1}C_{i,1}} \qquad \mathbf{B}(7,8) = \frac{1}{2C_{i,1}} \\
\mathbf{B}(8,1) &= \frac{1}{R_{i,3}C_{i,2}} \qquad \mathbf{B}(8,8) = \frac{1}{2C_{i,2}}
\end{aligned}
\tag{15}
$$

$$
\mathbf{c}(2) = \frac{1}{R_{c,3}} \qquad \mathbf{c}(4) = \frac{1}{R_{e,3}} \qquad \mathbf{c}(6) = \frac{1}{R_{f,3}} \qquad \mathbf{c}(7) = \frac{1}{R_{i,1}} \qquad \mathbf{c}(8) = \frac{1}{R_{i,3}} \tag{16}
$$

$$
\mathbf{d}(1) = \left(\frac{1}{R_{c,3}} + \frac{1}{R_{e,3}} + \frac{1}{R_{i,3}} + \frac{1}{R_{f,3}} + \frac{1}{R_{i,1}} + \frac{1}{R_w}\right) \qquad \mathbf{d}(2) = \frac{1}{R_w} \qquad \mathbf{d}(9) = 1.0 \tag{17}
$$

The state-space model is converted to a transfer function model as outlined in the previous section. The heat gains to the air at any time t are then

$$
\dot{Q}_{sh,t} = \sum_{k=0}^{8} \mathbf{S}_k^T \mathbf{u}_{t-k\Delta\tau} - \sum_{k=0}^{8} e_k \dot{Q}_{sh,t-k\Delta\tau} \tag{18}
$$

If the air temperature is controlled at a constant temperature, then the sensible cooling requirement ($\dot{Q}_{zs}$) is equal to the heat gain ($\dot{Q}_{sh}$). However, if the cooling system is off, then the heat gains cause a change in the temperature and internal energy of the air and any other internal mass not considered within the building structure (e.g., furnishings). Energy storage within the internal mass also occurs when the cooling system is on and the zone temperature is changing (e.g., during precooling or when the set point is not achieved). In general, an energy balance on the internal mass gives

$$
C_z \frac{dT_z}{dt} = \dot{Q}_{sh,t} - \dot{Q}_{zs,t} \tag{19}
$$

where C_z is the capacitance associated with internal zone mass (air and furnishings).

In order to determine the sensible cooling requirements and zone temperature for a given time step, three cases are considered: (1) zone temperature is maintained at a constant set point over the time step, (2) zone temperature is maintained at set points that vary between initial and final values over the time step, and (3) floating temperatures with the cooling system off or providing a specified zone sensible cooling rate.

In case 1, the left side of Equation (19) is zero and the sensible cooling requirement is equal to the heat gain. The heat gain is evaluated with Equation (18) using average values of the input variables for each time step. Thus, the cooling requirement represents an average value for the time step.

In case 2, it is necessary to integrate Equation (19) over each time step. In this case, the zone temperature is assumed to vary linearly in time over the time step between the specified initial and final temperatures. Furthermore, the heat-transfer gains are evaluated using the average zone temperature (and other inputs) over the time step.

Case 3 occurs when the estimated cooling requirement for case 1 or 2 is less than zero (equipment turns off) or greater than a limit (the cooling capacity). In order to estimate the "floating" temperature, the heat gain is assumed to be constant and evaluated at the average zone temperature over the time step and the zone sensible cooling rate is a constant (zero or a maximum capacity). This assumption leads to a linear variation in the zone temperature and the average and final temperatures are determined from Equations (18) and (19), and represented as

$$\bar{T}_{z,t} = \frac{\sum_{l=2}^{9} \mathbf{S}_0(l)\mathbf{u}_t(l) + \sum_{j=1}^{8} \mathbf{S}_j \mathbf{u}_{t-j\Delta\tau} - \sum_{j=1}^{8} e_j \dot{Q}_{sh,t-j\Delta\tau} - \dot{Q}_{zs,t} + 2\frac{C_z}{\Delta\tau} T_{z,t-\Delta\tau}}{2\frac{C_z}{\Delta\tau} - \mathbf{S}_0(1)} \tag{20}$$

$$T_{z,t} = T_{z,t-\Delta\tau} + 2\bar{T}_{z,t} \tag{21}$$

where $\mathbf{S}_0(l)$ is the l^{th} element of the $\mathbf{S}_0$ vector.

Model Training

The model training process begins with the collection of information associated with a physical description of the building. The information must include rough estimates of wall thicknesses, surface areas, and bounds on maximum and minimum thermal conductivity, specific heat, and density. The data are used to set bounds on the *R*s and *C*s to establish a region within the parameter space for a global direct search. In addition, the orientations of external walls and windows are required, along with surface areas and transmittances of windows and solar absorptances for external surfaces. These data are used in the calculation of absorbed and transmitted solar radiation and were not adjusted during model training in the current study. It is assumed that time-varying measurements of the sensible cooling requirement and inputs are available for the building for at least a week. The direct search algorithm determines good estimates of the model parameters that satisfy the constraints on parameters and the state-space representation and provide reasonable estimates of cooling requirements. Finally, a local nonlinear regression algorithm is used to determine optimal parameters that minimize errors between model predictions and measurements and satisfy the constraints.

Both the global and local training algorithms attempt to minimize a cost function that is the integrated root-mean-square error for a training duration, defined as

$$J = \sqrt{\frac{\sum_{k=1}^{N_{train}} (\dot{Q}_{d,k} - \dot{Q}_{zs,k})^2}{N_{train} - 1}} \tag{22}$$

The direct search algorithm evaluates the costs associated with a specified number of points within the bounded space to choose a starting point for the local optimizer. The points are generated using an algorithm presented by Aird and Rice (1977). The algorithm is tailored to problems in high-dimensional sets where bounds are available on the solution space and generates points within the bounded region that minimize the dispersion of the set. Figure 7 illustrates the manner in which the algorithm systematically places points so that the dispersion of the generated set is minimized. The four cases shown correspond to situations where the user specifies one, two, three, and four points, respectively.

At each generated point, the state-space representation is converted to a transfer function, the model is used to predict cooling requirements for the specified training data set, and the cost function is evaluated. The parameter values yielding the minimum cost are used as initial guess values for the local minimization algorithm.

The local regression process is the same as depicted in Figure 4 for the wall heat-transfer analysis. A Levenberg-Marquardt algorithm (Marquardt 1963; Meyer 1970) is applied to minimize the cost function of Equation (22).

The full optimization procedure can be summarized as follows: (1) bounds on the parameter space are established using a rough physical description of the building; (2) the number of points for the direct search is selected; (3) the points for the direct search are located within the parameter space using the algorithm of Aird and Rice (1977); (4) the costs are evaluated for all of the points; (5) the best point from the direct search is used as the starting point for the local minimization algorithm; and (6) the local optimization uses derivative information to identify optimal parameters. In selecting the number of points for the direct search there is a tradeoff between computational speed and resolution. The greater the number of points, the better the chance of identifying a global minimum. Because of the large number of parameters to be estimated, a relatively large number of points (e.g., 50,000) for the direct search is necessary to ensure a good result.

Evaluation of the Simulation

To develop and test the simplified building models, a detailed hourly simulation program, TRNSYS (Klein et al. 1990), was used to generate weather and incident solar data and provide "baseline responses" for building thermal behavior under specified control strategies.

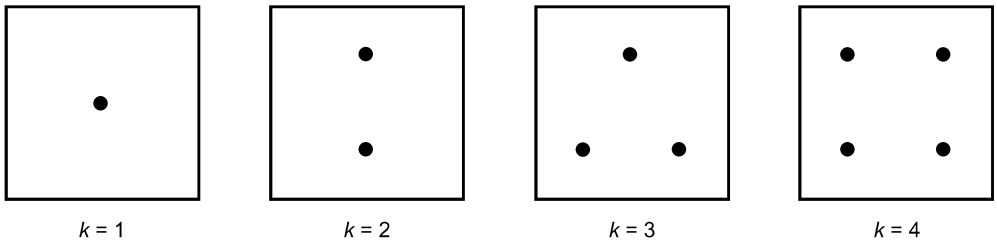

Figure 7. Systematic Generation of Points by Algorithm
Aird and Rice (1977)

The *Type 56 Multi-Zone Building* module of TRNSYS was used to model building thermal behavior. This is a very detailed model of a building that is built up from individual descriptions of wall layers, windows, internal gain schedules, etc. The model solves individual transient conduction through walls and considers long-wave radiation exchanges within the space. Model inputs include separate hourly heating and cooling set points and the model outputs the required heating or cooling rates necessary to maintain set points. For unoccupied periods, such as evenings or weekends, a high temperature set point is provided to the model. The cooling plant is off during these periods and the building temperature is allowed to "float" below the upper set point. If the floating temperature exceeds the high set point, the cooling equipment activates and provides cooling to maintain the set point. For the simulation studies on the sensible zone load, heating was not used and the cooling plant was assumed to have infinite cooling capacity.

Two small office buildings, termed block and frame, were considered in order to include the effect of building construction on the modeling errors. The behavior of a larger office building was investigated for the field evaluation considered in the next section.

The block building used heavy construction materials. The dimensions of the rectangular, single-story building were 75 ft by 100 ft (22.9 m by 30.5 m) with 10 ft (3.1 m) high walls. The exterior walls had 20% glass on all sides. The windows had a U-value of 0.7 Btu/h·ft^2·°F (3.98 W/m^2·K), a solar absorbtance of 0.05, a reflectance of 0.75, with outside and inside convection coefficients of 3.5 Btu/h·ft^2·°F (19.88 W/m^2·K) and 0.54 Btu/h·ft^2·°F (3.07 W/m^2·K), respectively. All of the window properties were considered to be time invariant. The building had approximately 1000 ft^2 (92.9 m^2) of internal wall area. An additional 5 lb/ft^2 (24.4 kg/m^2) was added to approximate internal mass due to office furniture and equipment. The specific heat of steel was used in conjunction with the total internal mass to achieve a lumped zone thermal capacitance of 4500 Btu/°F (8546 kJ/K).

The frame building used the same geometry and windows as the block building, but with relatively lightweight wall materials. The construction details for the walls used in the block and frame buildings are given in Table 2 and Table 3. The layer construction is ordered such that the first layer is the inside surface and the last layer is the outside surface, relative to the building's interior. The solar absorptances for all exterior surfaces were taken to be 0.5.

Occupancy and internal gain inputs were specified that are representative for commercial buildings. Both buildings were occupied from 7 A.M. to 5 P.M. on weekdays only and unoccupied during the other hours. Each was assumed to have one occupant per 100 ft^2 (9.29 m^2) of floor area and hence a total of 75 occupants. Equipment and lighting were assumed to be active one hour prior to occupancy. The weekday, occupied internal gains were 2.32 W/ft^2 (25 W/m^2) with 0.37 W/ft^2 (4 W/m^2) for people, 1.33 W/ft^2 (14.3 W/m^2) for lighting and 0.62 W/ft^2 (6.7 W/m^2) for equipment. The weekend and unoccupied gains were assumed to be 5% of those during occupancy. The internal gains were split into a convective and radiative component (lighting gains: 80% radiative and 20% convective; equipment gains: 20% radiative and 80% convective; occupant gains: 30% radiative and 70% convective). Both buildings were modeled as a single zone enclosed by external walls, internal walls, the ceiling, and the floor.

Bounds on material properties were specified based upon the known values given in Tables 2 and 3. Table 4 shows the bounds used for the block building. Similar bounds were established for the frame building. The known values of window transmittances and areas and exterior surface absorptances were used in the simplified model and were not adjusted during the training process.

Separate training and testing data were utilized in the simulated evaluations. The training period was varied between one and four weeks for June data. The testing period was one month in July. The simplified models were all trained using weather data for Boston. However, the accuracy of the trained models was tested in other locations and for different control strategies than those used for training. This approach tested the ability of the model to extrapolate to

Table 2. Block Building Construction Details

Wall	Layer	Thickness		Conductivity		Specific Heat		Density		Conv. Coef.	
		in	cm	Btu/ (h·ft·°F)	W/ (m·K)	Btu/ (lb_m·°F)	kJ/ (kg·K)	lb_m/ft^3	kg/m^3	Btu/ ($h·ft^2$·°F)	W/ (m^2·K)
External	Inside Air									0.54	3.1
	Gypsum	5/8	1.58	0.098	0.170	0.24	1.00	50	801		
	Insulation	1	2.54	0.017	0.029	0.29	1.21	2.2	35		
	Block	4	10.2	0.417	0.722	0.21	0.88	60	961		
	Brick	4	10.2	0.417	0.722	0.19	0.80	120	1922		
	Outside Air									3.5	19.9
Internal	Air									0.54	3.1
	Plaster	5/8	1.58	0.133	0.230	0.25	1.05	37	593		
	Block	4	10.2	0.417	0.722	0.21	0.88	60	961		
	Plaster	5/8	1.58	0.133	0.230	0.25	1.05	37	593		
	Air									0.54	3.1
Ceiling	Inside Air									0.54	3.1
	Ceiling Tile	1/2	1.27	0.033	0.057	0.14	0.59	23	368		
	Concrete	2	5.09	0.433	0.750	0.21	0.88	120	1922		
	Insulation	1	2.54	0.017	0.029	0.29	1.21	2.2	35.2		
	Roof	3/8	0.95	0.093	0.161	0.35	1.47	70	1121		
	Outside Air									3.5	19.9
Floor	Inside Air									0.54	3.1
	Carpet	1/2	1.27	0.03	0.052	0.33	1.38	35	561		
	Floor Tile	1/4	0.64	0.3	0.519	0.25	1.05	100	1602		
	Concrete	4	10.2	0.433	0.750	0.21	0.88	120	1922		
	Gravel	6	15.2	0.25	0.433	0.15	0.63	100	1602		

conditions beyond those used in the training process. The locations span different geographical regions and climates within the United States:

- Boston: Cooler to moderate ambient temperatures, low to moderate solar radiation
- Chicago: Moderate ambient temperatures, moderate solar loads, moderate load variations
- Miami: High ambient temperatures, low solar loads, high humidity
- Phoenix: High ambient temperatures, high solar loads, low humidity
- Seattle: Cooler to moderate temperatures, moderate loads with large variations

The controls strategies are described by the variation in zone temperature set points throughout the day. Figure 8 shows the zone temperature variations for the three control strategies used in the simulation studies. Further description of these strategies follows:

- **Night Setup**: This is a conventional strategy whereby a fixed temperature set point of 73°F (22.8°C) is maintained during occupancy. During unoccupied times, the set point is raised to 80°F (26.7°C). Typically the cooling equipment is inactive at night and active during the day. This strategy tends to minimize the total cooling requirement.
- **Light Precool**: The building is precooled for a few hours prior to occupancy using a zone set point of 67°F (19.4°C). The set point is raised to a fixed value of 73°F for the occupancy period.
- **Maximum Discharge**: This strategy uses a longer precool period with a set point of 67°F (19.4°C), maintains the low set point during the occupied off-peak period, and then raises the set point to the upper limit of the comfort range, 77°F (25°C), for the on-peak, occupied period. This strategy tends to minimize load requirements during on-peak, occupied times.

Table 3. Frame Building Construction Details

Wall	Layer	Thickness in	Thickness cm	Conductivity Btu/(h·ft·°F)	Conductivity W/(m·K)	Specific Heat Btu/(lb_m·°F)	Specific Heat kJ/(kg·K)	Density lb_m/ft^3	Density kg/m^3	Conv. Coef. Btu/($h·ft^2$·°F)	Conv. Coef. W/(m^2·K)
External	Inside Air									0.54	3.1
	Gypsum	1/2	1.27	0.098	0.170	0.24	1.00	50	801		
	Studs/Insul	3.5	8.9	0.034	0.059	0.23	0.96	7.3	117		
	Sheating	1/2	1.27	0.031	0.054	0.31	1.30	18	288		
	Siding	1/2	1.27	0.051	0.088	0.28	1.17	40	641		
	Outside Air									3.5	19.9
Internal	Air									0.54	3.1
	Gypsum	1/2	1.27	0.098	0.170	0.24	1.00	50	801		
	Studs/Insul	3.5	8.9	0.244	0.422	0.066	0.28	6.4	103		
	Gypsum	1/2	1.27	0.098	0.170	0.24	1.00	50	801		
	Air									0.54	3.1
Ceiling	Inside Air									0.54	3.1
	Ceiling Tile	1/2	1.27	0.033	0.057	0.14	0.59	23	368		
	Plywood	5/8	1.58	0.067	0.116	0.29	1.21	34	545		
	Insulation	1	2.54	0.017	0.029	0.29	1.21	2.2	35.2		
	Roof	3/8	0.95	0.093	0.161	0.35	1.47	70	1121		
	Outside Air									3.5	19.9
Floor	Inside Air									0.54	3.1
	Carpet	1/2	1.27	0.03	0.052	0.33	1.38	35	561		
	Concrete	4	10.2	0.433	0.750	0.21	0.88	120	1922		
	Gravel	6	15.2	0.25	0.433	0.15	0.63	100	1602		

Table 4. Material Property Bounds (Block Building) Used in Systematic Point Generation Algorithm

Wall	Minimum Conductivity Btu/(h·ft·°F)	Minimum Conductivity W/(m·K)	Maximum Conductivity Btu/(h·ft·°F)	Maximum Conductivity W/(m·K)	Min. Density-Spec. Heat Product Btu/(ft^3·°F)	Min. Density-Spec. Heat Product kJ/(m^3·K)	Max. Density-Spec. Heat Product Btu/(ft^3·°F)	Max. Density-Spec. Heat Product kJ/(m^3·K)
External	0.017	0.029	0.417	0.722	0.638	43	22.8	1529
Internal	0.133	0.23	0.417	0.722	0.925	62	12.6	845
Ceiling	0.017	0.029	0.433	0.750	0.638	43	25.2	1690
Floor	0.03	0.052	0.433	0.750	11.55	775	25.2	1690

The performance of the simplified model was evaluated using integrated root-mean-square errors and maximum errors, both normalized by the maximum load for the specific testing period. These errors are defined as

$$E_{rms} = \frac{100}{\dot{Q}_{d,m}} \sqrt{\frac{\sum_{k=1}^{N_{test}} \left(\dot{Q}_{d,k} - \dot{Q}_{zs,k}\right)^2}{N_{test} - 1}} \tag{23}$$

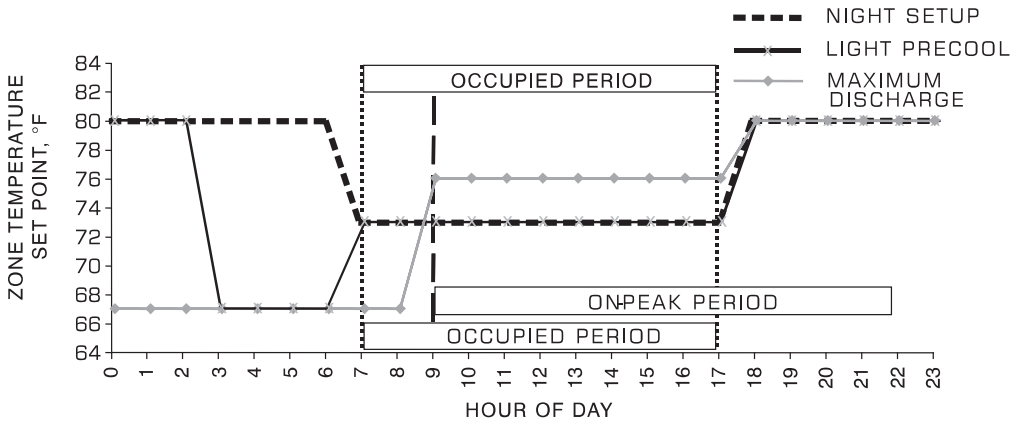

Figure 8. Control Strategies Used in Simulation Studies

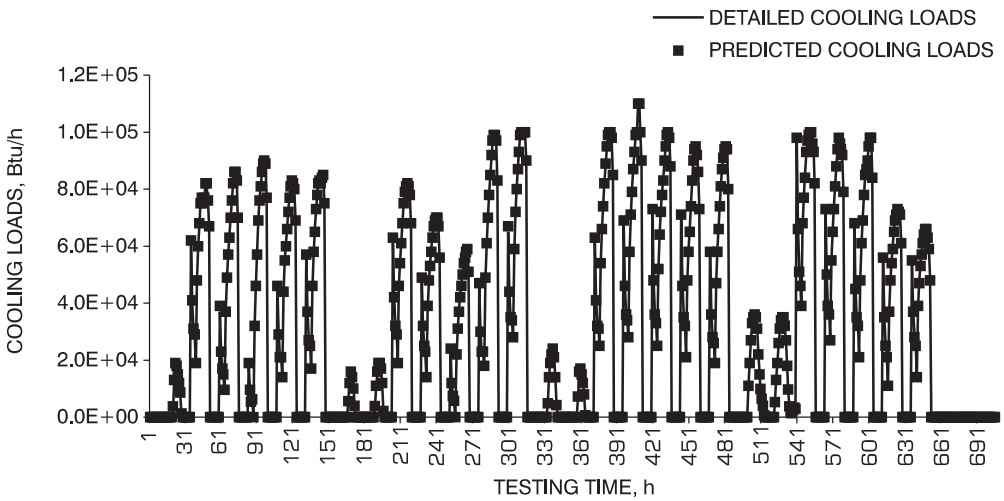

Figure 9. Comparison Between Sensible Cooling Requirements for Simplified and Detailed Model

(Block Building; Training: Maximum Discharge Strategy for 7 days in Boston; Testing: Night Setup Strategy for 30 days in Miami)

$$E_{peak} = \frac{100}{\dot{Q}_{d,m}}[\mathrm{Max}_{k=1,N_{test}}(\dot{Q}_{d,k}) - \mathrm{Max}_{k=1,N_{test}}(\dot{Q}_{zs,k})] \tag{24}$$

Figure 9 shows the sensible cooling requirements for the block building trained in Boston with the maximum discharge strategy for a period of seven days and tested using the night setup strategy in Miami for a one-month period. Figure 10 shows temperature predictions with specified cooling rates as inputs. The value of E_{rms} for the one-month testing period was 1.28% and the normalized peak error, E_{peak}, was 0.42%. For this case, the model extrapolated very well to another location and control strategy with only seven days of training. These results are indicative of the accuracy of the model when sufficient training data are available.

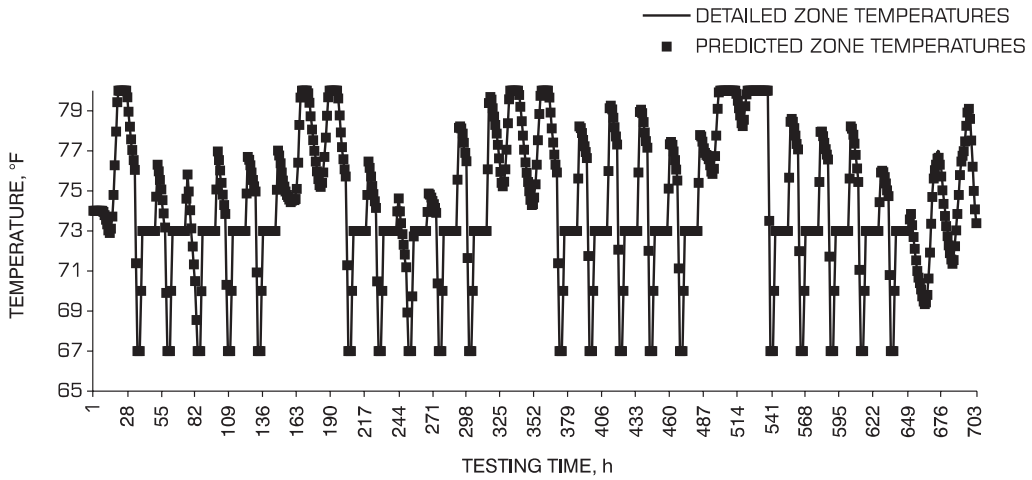

Figure 10. Comparison Between Zone Temperatures for Simplified and Detailed Model
(Block Building; Training: Maximum Discharge Strategy for 7 days in Boston;
Testing: Night Setup strategy for 30 days in Miami)

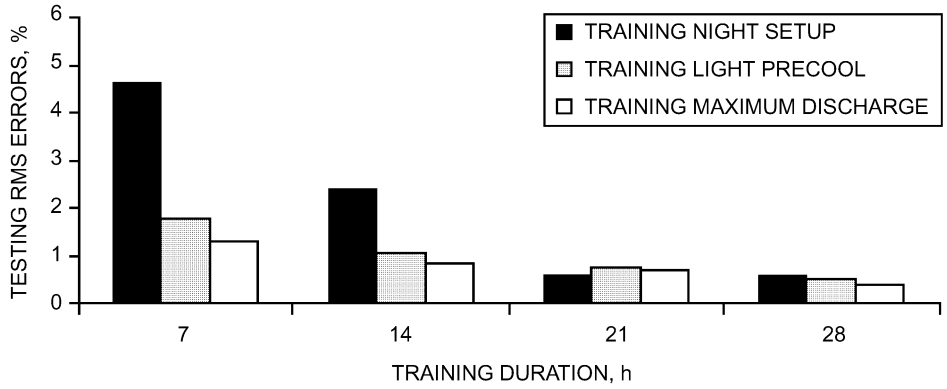

Figure 11. Comparison of Testing Errors for Different Training Strategies
(Block Building; Training: Boston; Testing: Maximum Discharge, Phoenix)

The accuracy of the simplified model depends upon the control strategies used for training and the duration of the training strategy. Figure 11 shows the effect of these two factors on model accuracy for a case where the testing strategy is maximum discharge. In this case, night setup required more training data to achieve the same accuracy as the other two strategies. About 7 to 14 days of training data were sufficient for the light precool or maximum discharge strategies, while 21 days would be more appropriate for use of night setup control for training. Maximum discharge was slightly better as a training strategy than the light precool strategy. In general, strategies with more set point variations provide a "richer" training set. Night setup is the worst case, since the set points are constant throughout the day. However, the differences associated with different training strategies were relatively small with 21 days of training data for this heavyweight building.

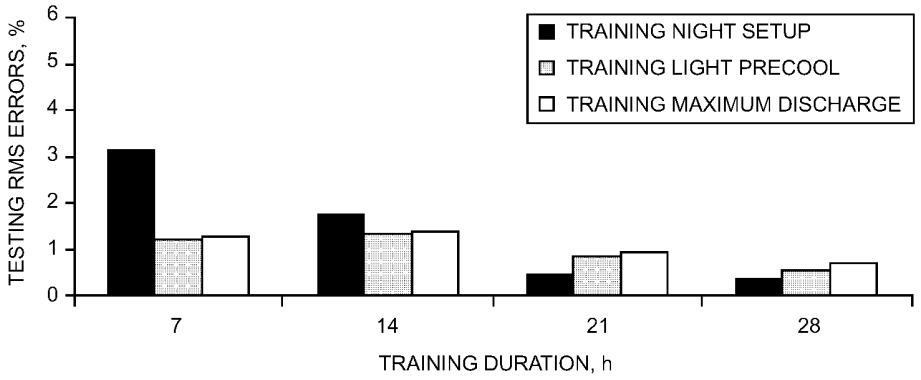

Figure 12. Comparison of Testing Errors for Different Training Strategies
(Block Building; Training: Boston; Testing: Night Setup, Phoenix)

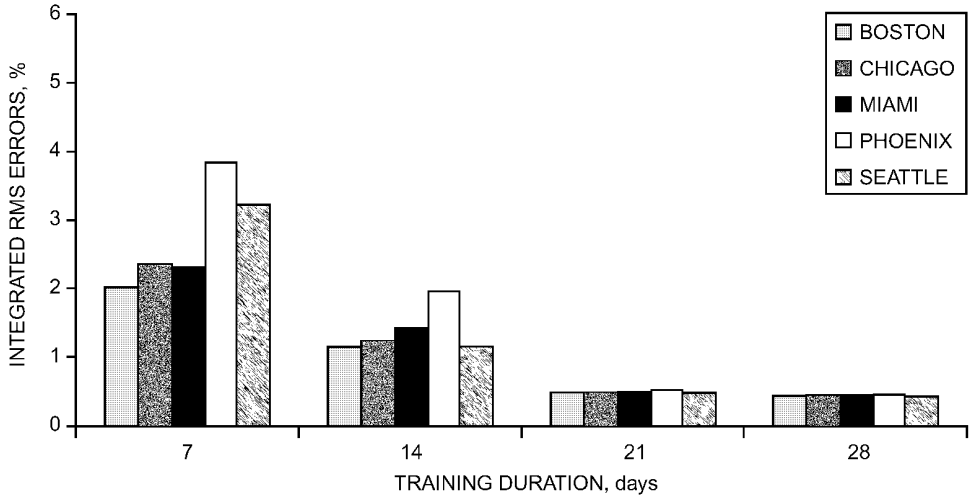

Figure 13. Comparison of Testing Errors for Different Geographical Locations and Different Training Periods
(Block Building; Training: Boston, Night Setup; Testing: Light Precool)

Model accuracy also depends upon the testing control strategy employed. Figure 12 shows results for a case where night setup was the testing strategy. In this case, night setup worked well as the training strategy with only about 14 days of training data.

Figure 13 shows the effect of testing location on model accuracy for the block building. In this case, the model was trained in Boston using night setup control and tested in the other locations with light precool. The model can be trained extremely well with 21 days of data. However, 14 days is probably sufficient. Again, less data would be required for use of a control strategy that has more variation in the zone temperature set points. With limited training data, the testing errors tend to be largest for testing data that are most different from those used to train the model. For Figure 13, the highest testing errors occurred in Phoenix, which generally

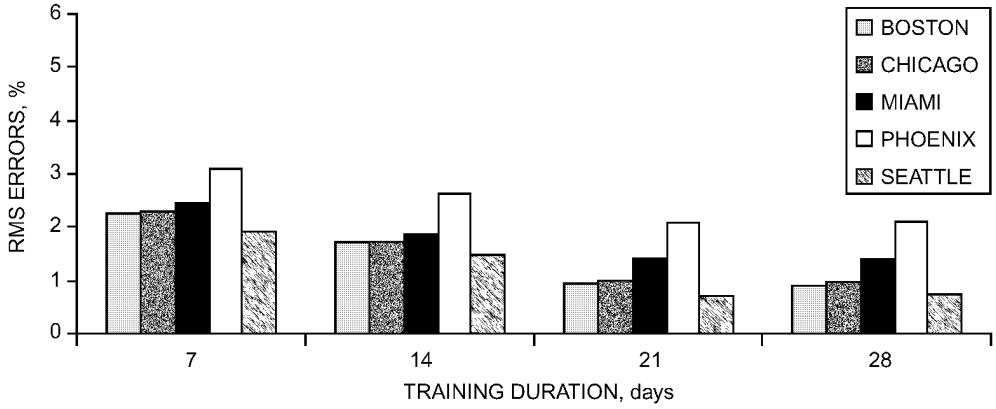

Figure 14. Comparison Between Testing Errors Across Different Geographical Locations and Across Different Training Periods
(Building: Frame; Training: Boston, Night Setup; Testing: Night Setup)

has much higher ambient temperatures and solar radiation than Boston. However, with sufficient training data, testing errors are relatively insensitive to testing location.

Figure 14 and Figure 15 show similar results for the frame building when night setup control was used for training. The results of Figure 14 are associated with night setup for testing, whereas Figure 15 was generated using the maximum discharge strategy for testing. The model accuracy for Boston is similar to that for the block building. However, the model did not do as well in extrapolating to other locations. In addition, the model accuracy is more sensitive to training duration and training and testing locations with this lighter weight structure. The frame building is more closely coupled to the ambient conditions than the block building, so that location differences are amplified. The performance would undoubtedly improve with longer training periods. However, a model trained with 21 days of data is probably sufficient. It is interesting to note that testing errors are actually greater for 28 days of training than for 21 days in Figure 15. For this case, the particular extra week of training data must have reduced the "richness" of the training data set.

Field Evaluation

The inverse building modeling approach was also tested using data collected from a commercial building located near Chicago, Illinois. Six weeks of data were available from the summer of 1997. Two weeks were used for training, while four weeks were used to test the model.

The building has four stories (three above ground) with a useable space of approximately 1.4 million ft^2 (130,000 m^2). The building has a large, central reception area with office space consuming most of the remaining area (see Figure 16). Office space is symmetrical on either side of the reception area. The building is constructed primarily of heavy weight concrete and has energy-efficient windows with excellent use of localized shading. Because much of the concrete structure is exposed internally, the building is a good candidate for using thermal mass control strategies.

A cooling plant provides chilled water to 16 air handling units within the building. These 16 air handlers each have supply and return variable-pitch, vane-axial fans for air distribution in the single duct, variable air volume (VAV) system. Data were logged using the building's energy management system and included zone temperatures for eight representative zones, ambient temperature and humidity, and air handler airflow rates, return air temperatures, and supply air temperatures.

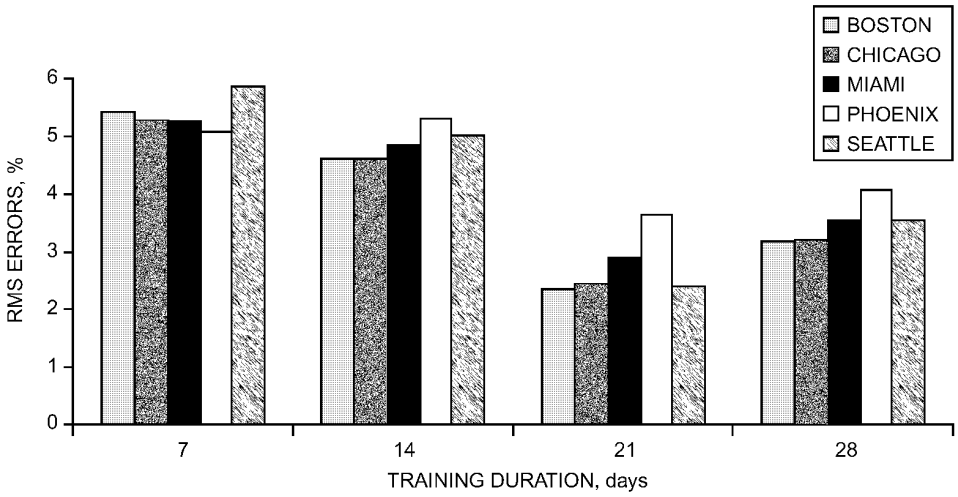

Figure 15. Comparison of Testing Errors for Different Geographical Locations and Across Different Training Periods
(Building: Frame; Training: Boston, Night Setup; Testing: Maximum Discharge)

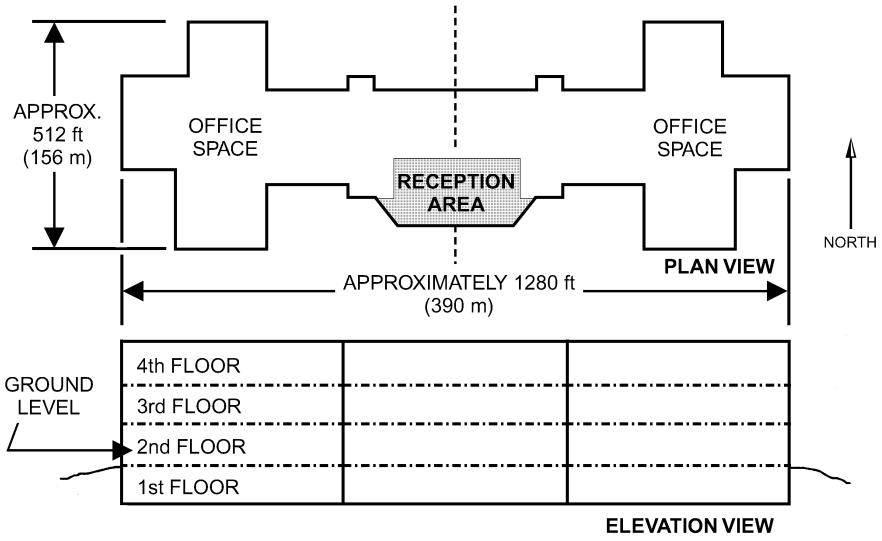

Figure 16. Layout of Field-Site Building

Pairs of air handlers share a common supply and return duct, so that the total sensible cooling requirements for the building were estimated from the data according to

$$\dot{Q}_{zs} = c_{p,air}\rho_{air}\sum_{i=1}^{8}[\dot{v}_{sup,pair,i}(T_{ret,i} - T_{sup,i})] \tag{25}$$

Solar data were not measured directly at the site, because the necessary equipment was not available. Instead, direct normal and horizontal solar radiation data collected from a nearby weather station (St. Charles) were used. The St. Charles weather station is approximately 15 miles southwest of the site and is monitored by the Water and Atmospheric Resources Monitoring Program under the guidance of the Illinois State Water Survey. The St. Charles station uses an Eppley pyranometer to measure solar radiation.

The entire test building was modeled as a single zone. A detailed description of the building layout and construction was not available and it was necessary to use several approximations to obtain initial parameter estimates. The wall areas and thickness, necessary for calculating initial values of the resistances and capacitances for the building network, were approximated using reasonable values available from building construction drawings. The total area of the internal walls was approximated as 10% of the floor area (for each floor). A horizontal skylight area was included which was approximated as 25% of the ceiling area. The wall solar absorptance was assumed to be 0.5, the effective transmittance of glass was taken as 0.10, and the window unit conductance was assumed to be 0.33 Btu/(h·ft^2·°F) [1.87 W/(m^2·K)]. Values for the convection coefficients on the inside and the outside of the different walls and the windows were assumed to be the same as those used for the simulated buildings.

The approximate values for surface areas, thicknesses, material properties, convection coefficients, and unit conductances were used to calculate initial *R*s and *C*s for the thermal circuit shown in Figure 6. The global search algorithm varied these parameters within bounds to determine initial values for the local regression algorithm. The bounds were established by specifying relative uncertainties for the surface areas, thicknesses, and material properties. A 50% uncertainity was established for areas and thicknesses. Table 5 gives the material property bounds used. The maximum and minimum limits on conductivity and the product of specific heat and density for each wall were taken as values corresponding to concrete and insulation. The initial values for solar properties (wall absorptance and window areas and transmittances) were not adjusted.

It was also necessary to make assumptions for some of the unmeasured inputs for both training and testing of the simplified model. The control strategy in place was a Light Precool strategy. However, the set point was not always maintained, so the measured temperature (calculated as the average of the eight measured building temperatures) was used to train and test the simplified model. Internal gains were modeled as a combination of the sensible gains from the occupants and the lighting and equipment. The occupant gains were calculated using a fixed number of occupants (3500), each with a heat loss of 75 W (ASHRAE 2001). The lighting and equipment gains were estimated to be 5 W/ft^2 (53.8 W/m^2) in the occupied period. The total internal gains were assumed to be 70% radiative and 30% convective. The unoccupied period internal gains were taken to be 10% of the total occupied period gains.

A single building temperature is a necessary input for training the simplified model. The representative building temperature was calculated by averaging eight zone temperatures recorded by the building's energy management and control system.

Table 5. Material Property Bounds for Global Search (Field Site Near Chicago, IL)

	Minimum Conductivity		Maximum Conductivity		Min. Density-Spec. Heat Product		Max. Density-Spec. Heat Product	
Wall	Btu/ (h·ft·°F)	W/ (m·K)	Btu/ (h·ft·°F)	W/ (m·K)	Btu/ (ft^3·°F)	kJ/ (m^3·K)	Btu/ (ft^3·°F)	kJ/ (m^3·K)
External	0.017	0.029	0.808	1.4	0.638	43	30.18	2024
Internal	0.017	0.029	0.808	1.4	0.638	43	30.18	2024
Ceiling	0.017	0.029	0.808	1.4	0.638	43	30.18	2024

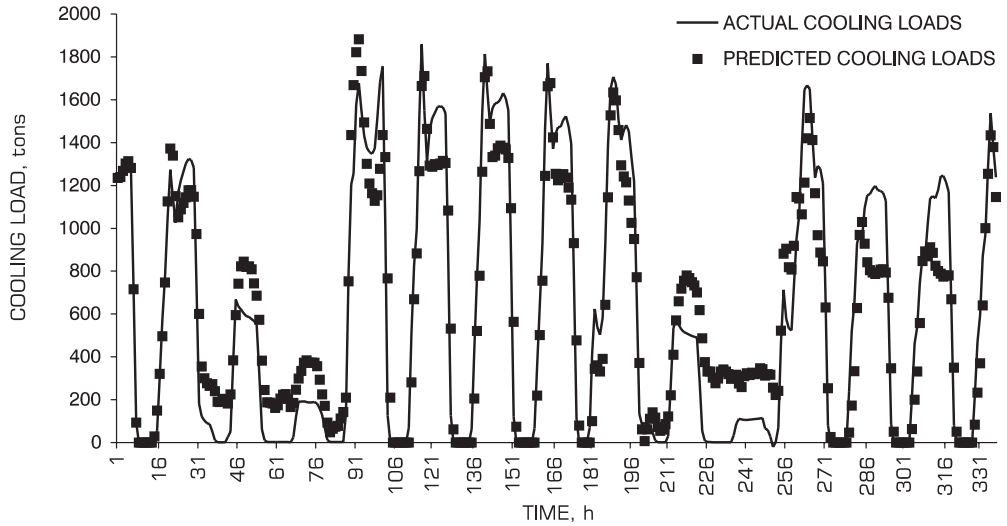

Figure 17. Comparison of Actual and Predicted Sensible Cooling Loads for Training Period
(Field Site Near Chicago, Illinois; 14 Days Training; Untuned Internal Gains)

Figure 17 shows results for sensible cooling loads for the field-site building for the training data set. The model appears to work reasonably well but tends to overpredict loads, especially during weekends and unoccupied hours. The relative RMS errors for training were 11.6% and are significantly higher than those obtained for the simulated data.

A sensitivity study was carried out to evaluate the impact of changes in model performance with changes in different parameters. It was found that the model errors were most sensitive to the magnitude of the internal gains. This is not surprising, since large buildings are generally dominated by internal gains. Furthermore, internal gains were not well known, especially during unoccupied times. The unoccupied internal gains were somewhat arbitrarily assumed to be 10% of the occupied values. Three additional parameters were introduced in the model to tune the internal gains schedule. The three parameters were multiplying factors for the gains during occupied, unoccupied, and weekend periods.

Figure 18 shows the sensible cooling load predictions for the modified model using the same 14 day training period used for the results of Figure 17. The relative RMS errors for training were reduced to 8.6%, a 3% improvement. The relative peak errors were 4%. Furthermore, the model did a much better job of predicting unoccupied and weekend loads.

The model was also evaluated using the separate four weeks of test data. Zone loads were predicted under the given temperatures and zone temperatures were estimated during periods of floating temperature. Comparisons of load and zone temperatures are shown in Figure 19 and Figure 20. The test comparisons are similar to the results for the training period. The error could probably be further reduced if more detailed occupancy information were available. For instance, people often worked after the normal hours and on weekends. However, the cooling requirements associated with these after-hour cooling requests were not considered properly in the model.

Conclusions

The inverse building modeling approach presented in this paper strikes a balance in terms of requirements for up-front building description information and measured data for training. If

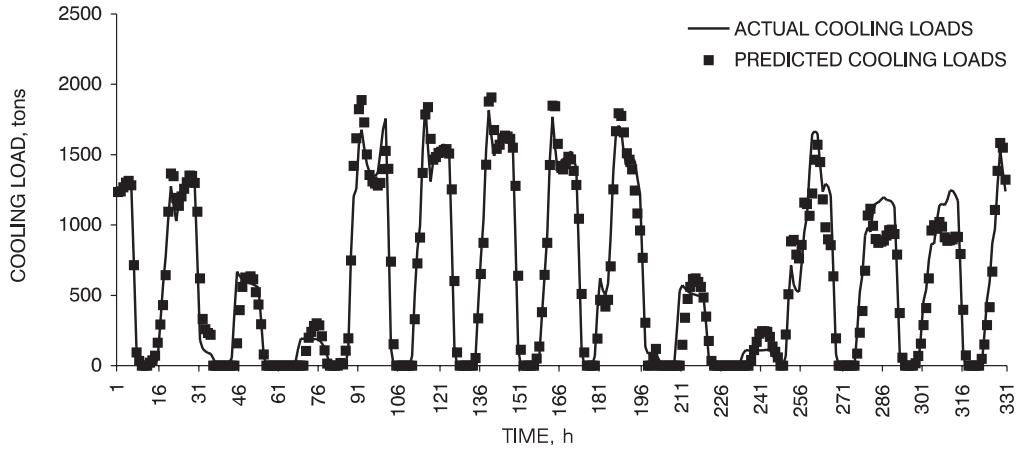

Figure 18. Comparison of Actual and Predicted Sensible Cooling Loads for Training Period
(Field Site Near Chicago, Illinois; 14 Days Training; Tuned Internal Gains)

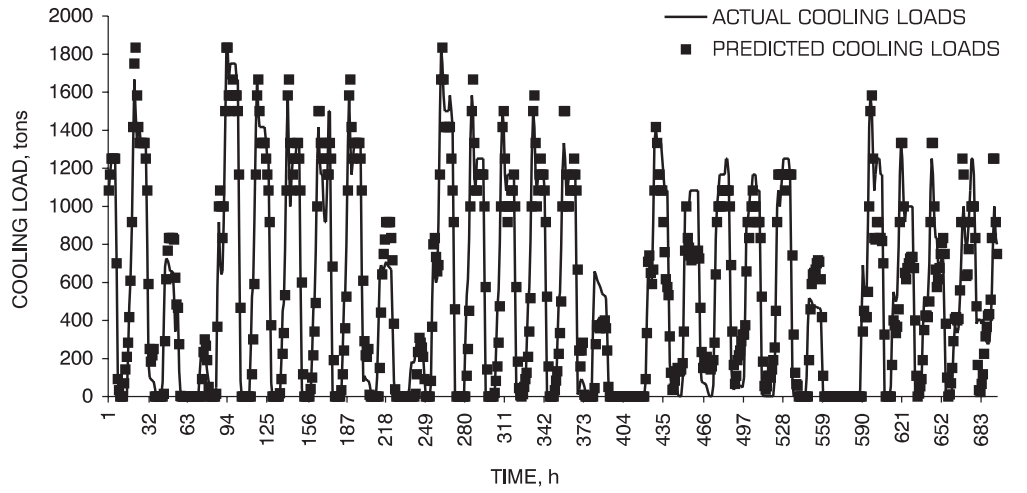

Figure 19. Comparison of Actual and Predicted Sensible Cooling Loads for Testing Period
(Field Site Near Chicago, Illinois; 14 Days Training; Tuned Internal Gains)

rich variations in zone temperatures are present, about a week of data is adequate to train an accurate building model. With limited zone temperature variations, about two to three weeks of data are necessary. Using test data generated from detailed simulations, the simplified model was able to match hourly loads to within about 2%. The model also extrapolated well to locations and strategies not used in the training process. However, all of these results used known inputs to the model (e.g., internal gains). In a real application, not all of the inputs would be measured or accurate. To address this issue, the inverse modeling approach was tested using measured data from a building located near Chicago, Illinois. Assumptions were made regarding unmeasured inputs and the model was trained using two weeks of data. The model was able to predict hourly cooling loads within about 9% for test data over a four-week period.

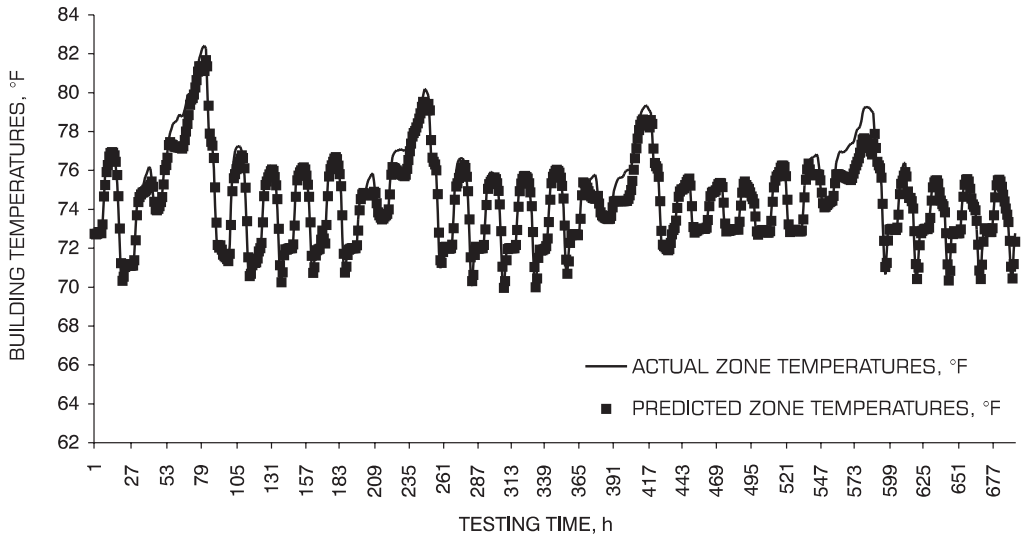

Figure 20. Comparison of Actual and Predicted Zone Temperatures for Testing Period
(Field Site Near Chicago, Illinois; 14 Days Training; Tuned Internal Gains)

ACKNOWLEDGMENTS

The work presented in this paper was sponsored by ASHRAE through TC 4.6. We appreciate the direction and patience of the project monitoring subcommittee: John Seem, Rich Hackner, and Frank Mayhew. We would also like to thank Lynn Jester for his efforts in supporting field testing.

NOMENCLATURE

$a_i, b_i, c_i,$ d_i, e_i	transfer function coefficients
A	constant coefficient matrix
B	constant coefficient matrix
c	constant coefficient vector
$c_{p,air}$	specific heat of air
d	constant coefficient vector
e_k	transfer function coefficient for the zone sensible load for k time steps prior to the current time t
E_{peak}	normalized peak error for test data
E_{rms}	normalized RMS error for test data
I	identity matrix
J	integrated root-mean-square error
k	simulation time step value
M, N	model order
N_{state}	number of state variables
N_{test}	number of hours in the test data set (= 744)
N_{train}	number of training points
$\dot{Q}_{d,k}$	actual (or detailed model) sensible cooling load at time step k
$\dot{Q}_{d,m}$	maximum actual (or detailed model) sensible load for test data
$\dot{Q}_{g,c}$	convective internal gains
$\dot{Q}_{g,r,c}$	radiative internal gains to the interior nodes of the ceiling/roof
$\dot{Q}_{g,r,e}$	radiative internal gains to the interior nodes of the external wall
$\dot{Q}_{g,s,k}$	total sensible internal gains at time step k
$\dot{Q}_{sh}$	instantaneous heat gain to the building air from all surfaces.
$\dot{Q}_{sol}$	total absorbed solar radiation on external surfaces
$\dot{Q}_{sol,k}$	total incident solar radiation on exterior surfaces at time step k
$\dot{Q}_{sol,w}$	solar radiation transmitted through windows

$\dot{Q}_{zs,k}$	sensible zone cooling load requirement at time step k
$\dot{Q}_{zs}$	building sensible cooling requirement
R	thermal resistance
$\mathbf{S}_k$	transfer function coefficients vector
T	temperature
$T_{a,k}$	ambient temperature at time step k
$T_{ret,i}$	return air temperature in air handler pair i
$T_{sup,i}$	supply air temperature in air handler pair i
$T_{z,k}$	zone temperature at time step k
$\mathbf{u}$	vector of inputs
$\mathbf{x}$	vector of state variables
y	output variable
ρ_{air}	density of air
τ	time
$\Delta\tau$	time step
$\dot{v}_{sup,pair,i}$	total volumetric air flow rate in air handler pair i

Additional Subscripts

a	ambient air
c	ceiling/roof
e	external
f	floor
g	ground
i	internal
w	window
z	zone air

REFERENCES

Aird, T.J. and J.R. Rice. 1977. Systematic Search in High Dimensional Sets. *SIAM Journal on Numerical Analysis* 14:296-312.

ASHRAE. 2001. *2001 ASHRAE Handbook—Fundamentals*. Atlanta: American Society of Heating, Refrigerating and Air-Conditioning Engineers, Inc.

Athienitis, A.K. and J. Shou. 1990. A General Method for Estimation of Building Transfer Functions from Detailed Thermal Models and Applications. *ASME International Computer Engineering Conference* 2:403-410.

Balaras, C.A. 1996. The Role of Thermal Mass on the Cooling Load of Buildings: An Overview of Computational Methods. *Energy and Buildings* 24(1):1-10.

Braun, J.E. 1990. Reducing Energy Costs and Peak Electrical Demand Through Optimal Control of Building Thermal Storage. *ASHRAE Transactions* 96(2):876-888.

Braun, J.E., K.W. Montgomery, and N. Chaturvedi. 2001. Evaluating the Performance of Building Thermal Mass Control Strategies. *International Journal of Heating, Ventilating, Air-Conditioning and Refrigerating Research* 7(4):403-428.

Crabb, J.A., N. Murdoch, and J.M. Penman. 1987. Simplified Thermal Response Model. *Building Services Engineering Research and Technology* 8(1):13-19.

Feuston, B.P. and J.H. Thurtell. 1994. Generalized Nonlinear Regression with Ensemble of Neural Nets: The Great Energy Predictor Shootout. ASHRAE Transactions 100(2):1075-1080.

Haghighat, F., P. Fazio, and R. Zmerneau. 1988. A Systematic Approach for Derivation of Transfer Function Coefficients of Buildings from Experimental Data. *Energy and Buildings* 12:101-111.

Iijima, M., K. Takagi, R. Takeuchi, and T. Matsumoto. 1994. A Piecewise-Linear Regression on the ASHRAE Time Series Data. *ASHRAE Transactions* 100(2):1088-1095.

Kawashima, M. 1994. Artificial Neural Network Backpropagation Model with Three-Phase Annealing Developed for the Building Energy Predictor Shootout. *ASHRAE Transactions* 100(2):1096-1103.

Klein, S.A., et al. 1990. TRNSYS. A Transient System Simulation Program, Version 13.1. Madison: Solar Energy Laboratory, University of Wisconsin.

MacKay, D.J. 1994. Bayesian Nonlinear Modeling for the Energy Prediction Competition. *ASHRAE Transactions* 100(2):1053-1062.

Marquardt, D. 1963. An Algorithm for Least-Squares Estimation of Nonlinear Parameters. *SIAM Journal on Applied Mathematics* 11:431-441.

Meyer, R., 1970. Theoretical and Computational Aspects of Non Linear Regression. *Non Linear Programming* J. Rosen, O. Mangasarian, and K. Ritter, Academic Press, New York, pp. 465-484.

Montgomery, K. 1998. Development of Analysis Tools for the Evaluation of Thermal Mass Control Strategies, M.S. Thesis, Herrick Laboratories, Purdue University, West Lafayette, Indiana.

Ohlsson, M., C. Peterson, H. Pi, T. Rognvaldsson, and B. Soderberg. 1994. Predicting Utility Loads with Artificial Neural Networks—Methods and Results from the Great Energy Predictor Shootout. *ASHRAE Transactions* 100(2):1063-1074.

Rabl, A. 1988. Parameter Estimation in Buildings: Methods for Dynamic Analysis of Measured Energy Use. *Journal of Solar Engineering* 110(1):52-66.

Seem, J.E., S.A. Klein, W.A. Beckman, and J.W. Mitchell. 1989. Transfer Functions for Efficient Calculations of Multi Dimensional Heat Transfer. *Journal of Heat Transfer—Transactions of the ASME* 111(1):5-12.

Stevenson, W.J. 1994. Predicting Building Energy Parameters Using Artificial Neural Nets. *ASHRAE Transactions* 100(2):1081-1087.